ORCA – Online Research @ Cardiff

Effects of Halo-substitution on 2′-Chloro-5′-halo-phenyl-1,2,3,5-dithiadiazolyl Radicals: A Crystallographic, Magnetic and EPR Case Study

Christos P. Constantinides,[†,§] *Emma Carter,*[‡] *Dana Eisler,*[†] *Yassine Beldjoudi,*[§] *Damien M. Murphy*[‡] *and Jeremy M. Rawson*[*,†,§]

[†]Department of Chemistry, The University of Cambridge, Lensfield Road, Cambridge, UK CB2 1EW

[‡]School of Chemistry, Cardiff University, Main Building, Park Place, Cardiff, UK CF10 3AT

[§]Department of Chemistry and Biochemistry, University of Windsor, 401 Sunset Avenue, Windsor, Ontario, Canada N9B 3P4

ABSTRACT: The syntheses and characterization of the aryl-substituted dithiadiazolyls, 2′-Cl-5′-X-C$_6$H$_3$CNSSN$^•$ [**1** (X = F), **2** (X = Cl), **3** (X = Br), **4** (X = I)] are described. In all four cases the radicals adopt distorted stacks of π*-π* dimers with inter-stack S⋯X contacts. In **1** (monoclinic *P2/c*) S⋯Cl contacts are manifested through a non-crystallographic 3-fold axis forming supramolecular trimers whereas the inter-stack S…X contacts in **2** (triclinic *P*-1), **3** and **4** (which form an isostructural pair, orthorhombic *P*na2$_1$) form supramolecular chains. While all the structures adopt π*-π* *cis*-oid dimer motifs, tuning the halogen modifies the intra-dimer S⋯S distance. Variable temperature SQUID magnetometry and X-band CW-EPR studies revealed the presence of a thermally accessible triplet state in all cases, with the singlet-triplet separation appearing in the order **1** > **2** > **3** > **4**, consistent with a reduction in the overlap integral with increasing intra-dimer S⋯S separation. Variable temperature structural studies on both **2** and **4** reveal a structural evolution from a distorted π-stack motif towards a regular π-stacked array on warming. This is particularly pronounced in **2** where the intermolecular S…S separations along the stacking direction converge on a regular 3.6 Å spacing at ambient temperature.

INTRODUCTION

1,2,3,5-Dithiadiazolyl radicals (DTDAs) have attracted considerable attention as building blocks for the construction of organic magnets[1,2] and more recently as paramagnetic ligands to *d*-block and *f*-block metal ions.[3-10] In the majority of cases these radicals associate in the solid state to form π^*-π^* dimers, although a number of monomeric DTDA radicals have been reported.[1,2,11-16] This dimerization is typically associated with short intra-dimer S···S contacts around 2.9 – 3.1 Å. Experimental electron density studies have revealed bond critical points (BCP) between S atoms in both the S–S bond and the intra-dimer S···S contact, although the electron density at the BCP between radicals is significantly less than that of the electron density at the S–S BCP, suggesting a significantly weaker interaction. Moreover the Laplacian is significant and positive and as Haynes points out, 'distinct from the values observed for covalent bonds".[17,18] These observations therefore raise questions about what is meant by a "bond" in these weakly associated dimer structures. A simple interpretation of the electronic structure of these systems is the formation of a closed-shell singlet (S_0) associated with efficient multi-center orbital overlap of the constituent singly occupied molecular orbitals (SOMOs). Indeed the assorted different modes of association (Fig. 1) all offer an in-phase bonding interaction between SOMOs which are of a_2 symmetry, leading to previous interpretations in terms of a 4-center, 2-electron bonding interaction between the S atoms or a 4-center, 6-electron dimer or even 14-electron σ/π-delocalized dimer description.[19-22]
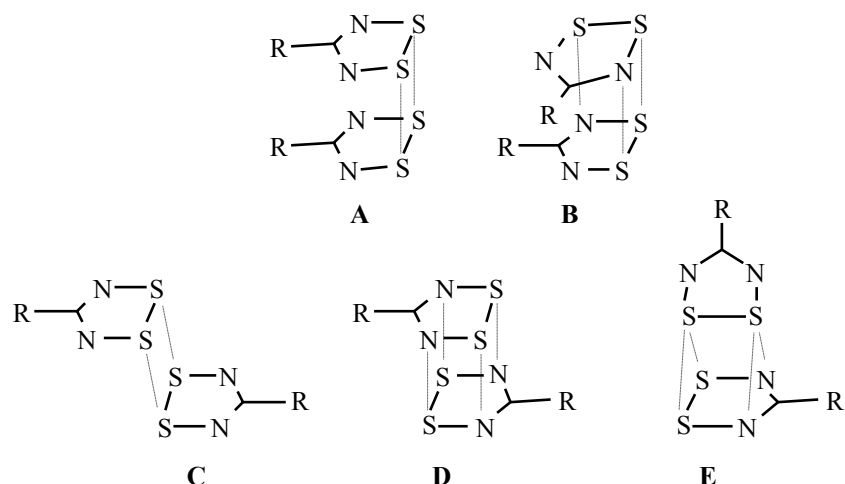
Figure 1. π^*-π^* modes of association in 1,2,3,5-dithiadiazolyl radicals.

Computational studies have proved challenging to locate these dimers as minima on the potential energy surface. Recent DFT calculations have successfully replicated the geometry and have not only shown the importance of dispersion forces in stabilizing these π^*-π^* aggregates but also identified significant diradical character (S_1) in the ground state.[23-25] These studies indicate that this dimerization process lies somewhere on the continuum between two independent radicals ($S = \frac{1}{2}$) and a multi-centre bond ($S = 0$). Orbital overlap between the two singly occupied molecular orbitals gives rise to bonding (φ) and antibonding combinations (φ^*), where the energy gap (ΔE) between them is sensitive to the overlap integral. If ΔE is large then a 'conventional' closed-shell singlet configuration (S_0) is anticipated (Fig. 2a). However, if the orbital overlap is reduced then ΔE becomes comparable with the inter-electron repulsion term P, associated with placing two electrons in the same orbital (φ). In this case the open shell configurations S_1 and T_1 (Fig. 2b and 2c) become energetically favored and the dimer is destabilized. Computational studies reflect some admixing of the excited S_1 term into the S_0 ground state affording some diradical character,[23,24] and experimental studies by us[26-28] and

others[23,29] on DTDA radicals and related members of this family of heterocyclic radicals have identified the presence of low-lying thermally accessible triplet excited state configurations (T_1). Chemical approaches to tailor the orbital overlap will modify ΔE and permit a systematic experimental study of the electronics occurring during this bond-forming process.

(a) $\Delta E > P$ (S_0)   (b) $\Delta E < P$ (S_1)   (c) $\Delta E < P$ (T_1)
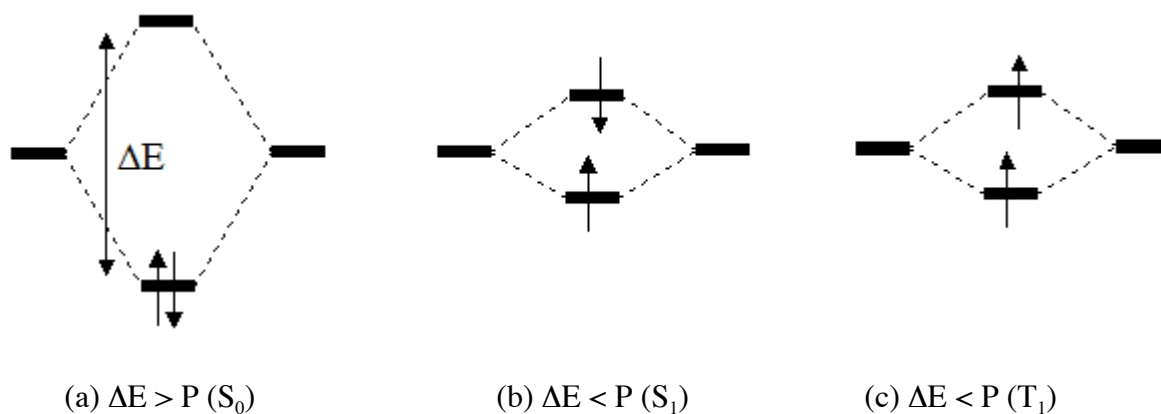
Figure 2. Possible electronic configurations arising out of π^*-π^* dimer formation; (a) a closed shell singlet (S_0) when $\Delta E > P$; (b) open shell singlet (S_1) and (c) open shell triplet (T_1) states when $\Delta E < P$.

In this paper we examine the series of structures of formula $2'$-Cl-$5'$-X-$C_6H_3CNSSN^\bullet$ [**1** (X = F), **2** (X = Cl), **3** (X = Br), **4** (X = I)] (Scheme 1) which all adopt π-stacked motifs and utilize the halogen at the $5'$-position to tune the orbital overlap between DTDA radicals. We probe the structures of **1** - **4** through single crystal X-ray diffraction and their magnetic properties through solid-state SQUID magnetometry and continuous wave (CW)-EPR studies. These studies allow us to tailor the overlap integral within the dimer and see how this is manifested in the resultant electronic structure of these radicals. We go on to examine the thermal evolution of the solid state structure which reveal a second order progression towards a regular π-stacked motif.
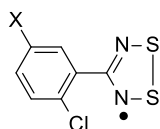
1: X = F; **2**: X = Cl; **3**: X= Br; **4**: X = I

Scheme 1

EXPERIMENTAL SECTION

All reagents (Li[N(SiMe$_3$)$_2$], Ag powder and benzonitriles) were used as received without any further purification. SCl$_2$ was prepared by chlorination of S$_2$Cl$_2$ according to the literature method.[30] All the reactions carried out and the compounds prepared were air and moisture sensitive, therefore inert atmosphere techniques were applied throughout the work. All glassware was pre-dried with a heat gun prior to use. Reactions were carried out in standard Schlenk apparatus under a nitrogen atmosphere (in-house supply dried by passing through a P$_4$O$_{10}$ column) using standard vacuum double-manifold techniques. The air and moisture sensitive materials were handled under nitrogen in a Saffron Scientific Beta-range glove box fitted with molecular sieve and copper catalyst columns for the removal of water and oxygen respectively. Et$_2$O was freshly distilled off Na prior to use and THF freshly distilled off CaH$_2$ under argon. Carbon, nitrogen and hydrogen analyses were carried out on an Exeter CE-440 Elemental Analyser. Samples of ~ 2 mg were sealed into pre-weighted capsules under nitrogen in the glove box. Electron ionization (+EI) mass spectra were obtained on a Bruker Daltonics FT-ICR Bio-Apex II using anhydrous THF as the liquid phase for radicals **2** – **4** and on Varian 1200L Quadrupole MS spectrometer for radical **1**. Quoted unit mass data reflect different isotopomers for the molecular ion peaks with greater than 10% relative intensity. IR spectra were recorded on

a Perkin-Elmer Spectrum-One FT-IR instrument for radicals **2 – 4** and on Bruker Alpha-P FT-IR for radical **1**. The EPR spectra were recorded on a CW X-band (~ 9 GHz) Bruker EMX spectrometer operating at 100 kHz field modulation, 10 mW microwave power and fitted with a high sensitivity cavity (Bruker ER 4119HS). The spectrometer is equipped with a variable temperature unit to allow measurements to be performed at temperatures ranging from 120 to 298 K. The low temperature (10 – 140 K) CW-EPR spectra were recorded on an X-band Bruker ESP300e series spectrometer using 12.5 kHz field modulation, 2.5 mW and fitted with a Bruker CW ENDOR cavity (EN801) equipped with an Oxford instrument ESR 900 continuous flow He cryostat. The *g* values were determined using a DPPH standard. A small quantity of the polycrystalline DTDA samples were loaded into high-quality suprasil EPR tubes for measurement. EPR simulations were performed using the Easyspin toolbox for Matlab.[31] Variable-temperature magnetic susceptibility data were recorded on a Quantum Design MPMS-XL SQUID magnetometer employing a magnetic field of 0.5 T in the temperature region 5 – 300 K. Single crystal X-ray diffraction was undertaken using single crystals mounted on the end of glass fibers using perfluoro-polyether oil and XRD data were collected on a Nonius Kappa CCD diffractometer, utilizing monochromatic Mo-Kα radiation (λ = 0.71073 Å for radicals **1 – 4** respectively). The temperature was controlled using an Oxford Cryosystems cryostream device. Structures were solved using direct methods and refined using full matrix least squares methods on F^2 using SHELXTL v6.12.[32] Graphics were prepared using Mercury.[33] Structural data for the three new compounds **1**, **3** and **4** have been deposited with the Cambridge Crystallographic Data Centre (CCDC deposition numbers 1517289 – 1517291). Additional variable temperature structural studies on **2** and **4** were undertaken from 140 K to room temperature on a Bruker D8 Venture APEX-III diffractometer with a Photon 100 CCD detector. The temperature was

controlled using an Oxford Cryosystems cryostream device. In these studies a single crystal of **2** or **4** was initially cooled to 140 K and full data sets were measured over a range of temperatures up to room temperature. For **4** data were collected using Mo-Kα radiation but Cu-Kα radiation was implemented for the small crystal of **2** utilized in these studies. Compound **2** was a non-merohedral twin and details of the processing and refinement of these data are available in the ESI. These temperature dependent structures have also been deposited with the CCDC (CCDC deposition numbers CCDC 1537428-1537434 and 1537436-1537439).

General procedure

The dithiadiazolyl radicals **1 – 4** were prepared from the corresponding benzonitriles according to standard synthetic methods[26-28] and were purified by vacuum sublimation: In a typical reaction 2-chloro,-5-halo-benzonitrile (10.0 mmol) was stirred overnight with $Li[N(SiMe_3)_2]$ (1.67 g, 10.0 mmol) in Et_2O (30 mL). Subsequent slow addition of SCl_2 (2.1 mL, 21 mmol) at 0 °C yielded an immediate bright yellow precipitate, which was stirred for a further 3 h at room temperature prior to filtration and drying *in vacuo*. THF (20 mL) and Ag powder (1.5 g, 14 mmol) were added and the suspension stirred for 18 h at room temperature to afford a very dark purple-black solution. The crude product was dried *in vacuo* and purified by vacuum sublimation. Yields were not optimized for these magneto-structural studies.

Compound **1**: Sublimation (75 – 50 °C, 10^{-1} Torr) yielded black needles (0.131 g, 6%). IR (4000 – 450 cm^{-1}): 3089vw, 3045vw, 1607m, 1582m, 1475m, 1422m, 1347m, 1258m, 1203m, 1134w, 1106m, 1055m, 974m, 879m, 826s, 777s, 717w, 669w, 660w, 641s, 553m, 511m, 481m, 451w. Anal. Found (calc. for $C_7H_3ClFN_2S_2$): C, 35.7 (36.0); H, 1.4 (1.3); N, 11.8 (12.0). MS (EI+): 235 (M^+, 44%), 234 (M^+, 12), 233 (M^+, 100).

Compoundd **2** has been reported previously.[26] Vacuum sublimation (115 – 80 °C, 10^{-1} Torr) afforded dark green lustrous plates of **2** (0.79 g, 32%). IR (4000 – 650 cm^{-1}): 3087vw, 3037vw, 1587w, 1557w, 1469s, 1402m, 1343s, 1263w, 1229w, 1154w, 1102s, 1071w, 1050s, 937m, 886m, 824s, 805s, 780s, 765m, 717w, 666w. Anal. Found (calc. for $C_7H_3Cl_2N_2S_2$): C, 33.9 (33.6); H, 1.3 (1.2); N, 11.3 (11.2). MS (EI+): 253 (M$^+$, 17), 251 (M$^+$, 74), 249 (M$^+$, 100).

Compound **3**: Sublimation (115 – 75 °C, 10^{-1} Torr) afforded black rods (0.685 g, 23%). IR (4000 – 650 cm^{-1}): 3089w, 1681vw, 1588m, 1552w, 1471m, 1429w, 1386m, 1355m, 1297w, 1249w, 1226w, 1124m, 1102s, 1048w, 1030m, 938vw, 885m, 863m, 825m, 805m, 779s, 769s, 737s, 718s, 661s. Anal. Found (calc. for $C_7H_3ClBrN_2S_2$): C, 24.7 (24.6); H, 1.0 (0.9); N, 8.2 (8.2). MS (EI+): 297 (M$^+$, 33%), 295 (M$^+$, 100), 293 (M$^+$, 75).

Compound **4**: Sublimation (125 – 75 °C, 10^{-1} Torr) afforded black blocks (0.68 g, 20%). IR (4000 – 650 cm^{-1}): 3068vw, 1682w, 1618w, 1588w, 1464m,br, 1393m, 1338m, 1249m, 1221m,br, 1124m, 1103m, 1079m, 1046s, 920w, 886m, 813s, 778s, 738s, 718s, 660m. Anal. Found (calc. for $C_7H_3ClIN_2S_2$): C, 24.7 (24.6); H, 1.0 (0.9); N, 8.2 (8.2). MS (EI+): 343 (M$^+$, 30%), 341 (M$^+$, 69).

X-ray diffraction

Identification of the 'correct' unit cell (Table 1) in all cases proved extremely problematic due to significant pseudo-symmetry and, in the case of **2**, twinning. In particular, cells with a halving of the crystallographic axis corresponding to the π-stacking direction (*ca.* 7.2Å) provided adequate solutions which appeared as a 'regular' π-stacked structure. Such problems have been identified previously.[26,34] For example the highest symmetry setting for **1** was *C2/c* with *b* = 3.6 Å, three molecules in the asymmetric unit and a regular spacing of radicals parallel to the crystallographic *b*-axis. However, an initial refinement indicated that the S atoms unexpectedly

exhibit markedly elongated U_{ij} with thermal displacement parameters larger than those for N, indicating potential static or dynamic disorder. Conversely, refinement within a super-cell (monoclinic $P2/c$ with b = 7.2 Å) revealed an ordered structure with 6 molecules (3 dimers) in the asymmetric unit with much improved thermal parameters. Similarly, the structures of **3** and **4** were initially solved in $P\text{ca}2_1$ with two molecules in the asymmetric unit but with distorted U_{ij} parameters. Subsequent refinement in $P\text{na}2_1$ with a doubling of the b-axis provided a solution with four crystallographically independent molecules with much improved thermal parameters. More detailed variable temperature studies on **2** and **4** as representative of this series are discussed later.

Table 1   Crystallographic data for **1 – 4**. Data for **2** reproduced from reference 26.

| Compound	1	2	3	4
Formula	$C_7H_3ClFN_2S_2$	$C_7H_3Cl_2N_2S_2$	$C_7H_3ClBrN_2S_2$	$C_7H_3ClIN_2S_2$
FW (g/mol)	233.68	250.13	294.59	341.58
Crystal System	Monoclinic	Triclinic	Orthorhombic	Orthorhombic
Space group	$P2/c$	P-1	$P\text{na}2_1$	$P\text{na}2_1$
a/Å	20.9551(2)	7.3271(2)	20.0576(2)	20.3822(5)
b/Å	7.21560(10)	10.3563(3)	7.47520(10)	7.8030(2)
c/Å	35.3686(5)	24.6666(7)	24.6660(3)	24.5317(6)
α/°	90	88.096(2)	90	90
β/°	106.8850(6)	81.458(2)	90	90
γ/°	90	77.0090(10)	90	90
V/Å^3	5117.31(11)	1803.60(9)	3698.29(8)	3901.58(17)
T/K	180(2)	180(2)	240(2)	180(2)
θ range (°)	1.02 < θ < 25.03	1.02 < θ < 25.35	1.02 < θ < 31.51	1.00 < θ <27.88
Z	24	8	16	16
D_c (g/cm^3)	1.820	1.842	2.116	2.326
μ(Mo-Kα)/mm^{-1}	0.898	1.127	5.133	3.934
R_{int}	0.0661	0.0395	0.0678	0.0596
R_1 ($I > 2\sigma(I)$)	0.0527	0.049	0.0407	0.0464
wR_2 (all data)	0.0959	0.112	0.0784	0.1141
S (all data)	1.046	1.050	1.111	0.912
Min/max	+0.37	+0.41	+0.55	+2.13
e^- density/ e^-Å^{-3}	-0.37	-0.47	-0.56	-0.99

RESULTS AND DISCUSSION

The radicals **1 – 4** were prepared according to standard synthetic methodologies[21-23] and isolated

in non-optimized yields of 6 – 32%, providing adequate material for structural, magnetic and

EPR studies on each derivative. The isotope distribution patterns for **1 – 4** provided diagnostic

mass spectra. Crystalline samples of all radicals **1 – 4** were carefully scrutinized for the presence

of different polymorphs but, in our hands, each compound appeared phase pure.

Crystal Structures

Structure of 1. Radical **1** crystallizes in the monoclinic space group *P*2/c with six molecules

(three crystallographically independent dimers) in the asymmetric unit. Within each of the six

independent molecules, the presence of the *ortho*-chlorine induces a significant twist between

each aryl ring and the dithiadiazolyl ring (25.02 – 28.40°, mean 26.94°). The three *cis*-oid dimers

are located about a non-crystallographic 3-fold axis (Fig. 3). The intra-dimer S···S contacts range

from 3.154(2) – 3.235(2) Å affording a π^*-π^* 'pancake' bonding interaction.[35] These dimers

form a distorted π-stack parallel to the crystallographic *b* axis with inter-dimer close contacts

along the stacking direction somewhat longer [4.036(2) – 4.097(2) Å] than the intra-dimer

distances but within the sum of the van der Waals radii perpendicular to the ring plane (4.06 Å).[36]

The intra-stack Cl…Cl contacts are more regularly spaced, ranging from 3.572(1) – 3.661(1) Å.

All the intra- and inter-dimer S…S and Cl…Cl contacts, as well as inter-stack S…Cl contacts,

for **1** are tabulated in the ESI (Table S.3).

These stacks are linked through a series of S···Cl interactions [3.234(2) – 4.274(2) Å], with the

majority within the van der Waals radii of S and Cl (3.55 Å).[36] DTDA radicals exhibit a strong

propensity to form in-plane S⋯Cl contacts to both covalent chlorine in chloro-aryl DTDA radicals[26,37] as well as to chloride counter-ions in dithiadiazolylium chloride salts.[38-48] The S⋯Cl contacts in **1** (3.234(2) – 3.747(2) Å) are close to those observed to other covalently bonded chlorine atoms [*c.f.* S⋯Cl at 3.385(5) and 3.521(5) Å in (*p*-ClC$_6$H$_4$CNSSN)$_2$ (WIMNAH)].[37] These S⋯Cl interactions link π-stacked columns together to form triangular columns (Fig. 3). Within these columns each dimer is vertically offset from other dimers so as to permit additional longer S…Cl contacts to the next dimer 'up' or 'down' the stack.
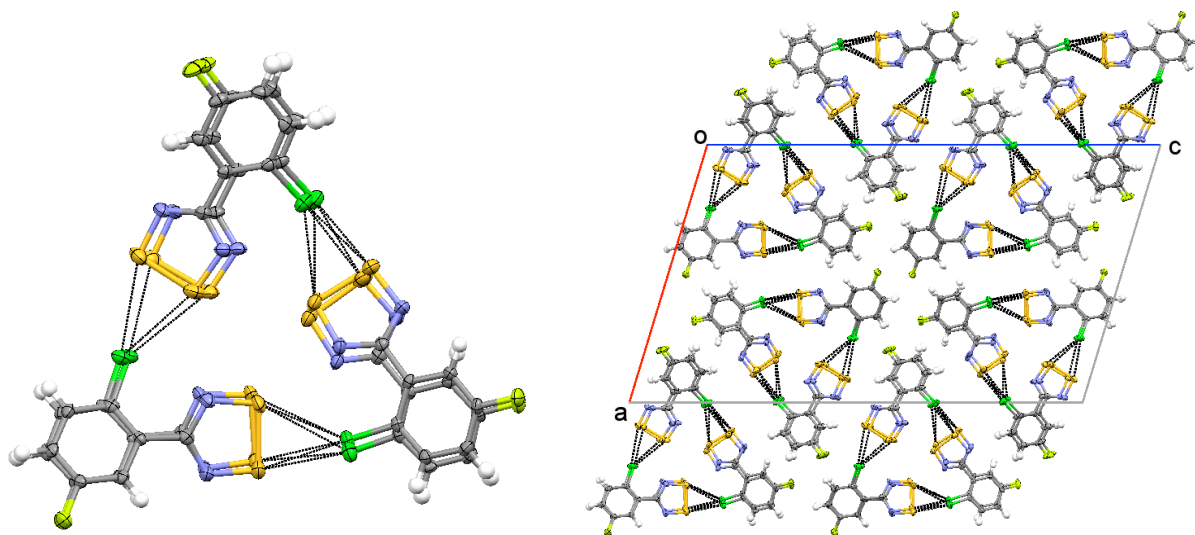
Figure 3. (left) Asymmetric unit of **1** illustrating the structure-directing S…Cl contacts which form supramolecular triangles; (right) packing of triangles in the *ac* plane.

These trimers of dimers which comprise the asymmetric unit of **1** are then further linked in the *ac* plane by a series of C-H⋯N [2.632(4) – 2.807(4) Å] and C-H⋯F [2.604(2) – 2.751(2) Å] contacts (Fig. 3) which are not dissimilar to those reported previously for a range of fluorophenyl-dithiadiazolyl radicals.[49]

Structure of 2. The structure of **2** (MEJZIL) has been reported previously[26] but it is instructive to provide a short description here in relation to **1**, **3** and **4**. Radical **2** crystallizes in the triclinic space group *P*-1 with two *cis*-oid dimers in the asymmetric unit with torsion angles between DTDA and aryl rings in the range 26.67 – 28.19° (mean 27.51°). At 180 K the intra-dimer S⋯S distances [3.156(6) – 3.268(5) Å] are notably longer that those observed in other *cis*-oid dimers [mean 3.09(6) Å] indicative of some weakening of the π^*-π^* dimer interaction but comparable to **1** [3.154(2) – 3.235(2) Å]. These dimers form a distorted π-stack parallel to the crystallographic *a*-axis with inter-dimer S⋯S contacts significantly longer [4.075(5) – 4.185(6) Å] than the intra-dimer contacts. Conversely the dichlorophenyl rings are almost evenly spaced [3.619(4) – 3.710(4) Å] consistent with the preferred "β-sheet" structure [3.77 – 4.02 Å].[50] Like **1**, **2** also exhibits close in-plane S⋯Cl contacts between neighboring dimer pairs [3.377(4) – 3.706(4) Å, mean 3.563 Å] but, in contrast to **1**, these contacts are now to the Cl atom at the 5′-position. Instead of forming discrete supramolecular trimers, these contacts link dimers into chains parallel to the crystallographic *b*-axis (Fig. 4). A network of close inter-chain interactions
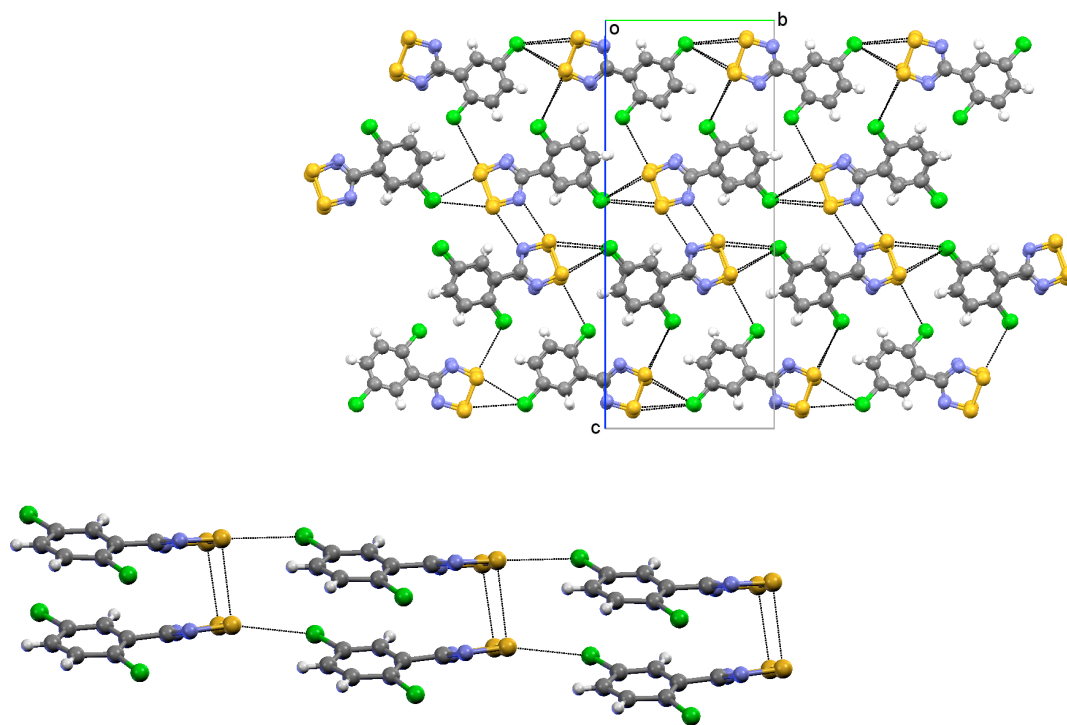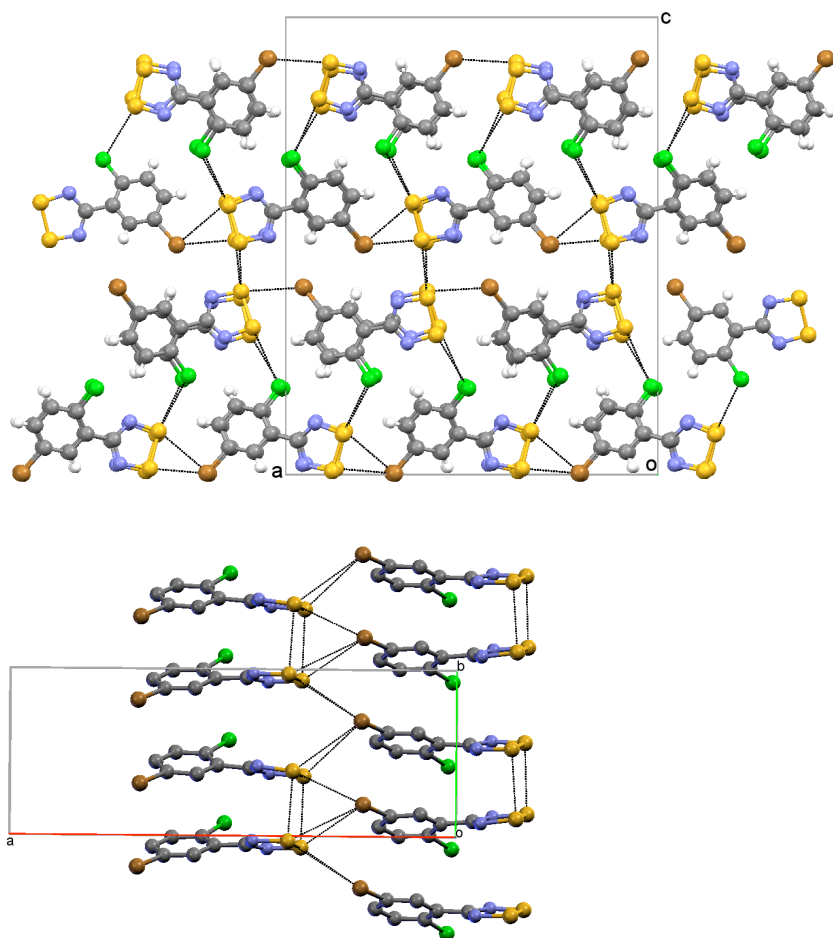
Figure 4. (top) solid state structure of **2** viewed perpendicular to the crystallographic *bc* plane, highlighting intermolecular S⋯Cl and S⋯N contacts; (bottom) detail of the inter-stack chain-forming S…Cl contacts.

is also observed. Amongst these the S⋯N contacts [3.288(9), 3.390(9) Å] link dimers in adjacent antiparallel chains and are a common motif in dithiadiazolyl chemistry.[51,52] The combination of in-plane intra-chain S…Cl and in-plane inter-chain S…N contacts forms a lamellar ribbon (Fig. 4). Additional inter-ribbon contacts comprise a bifurcated set of C-H⋯Cl [2.854(3), 2.911(3) Å] as well as C-H⋯N [2.726(1) Å] and S⋯Cl [3.275(5) and 3.648(4) Å] contacts. These lead to a vertical offset between ribbons.

Structure of 3. Radical **3** crystallizes in the orthorhombic space group $Pna2_1$ with four crystallographically independent molecules in the asymmetric unit. In radical **3**, like both **1** and **2**, the presence of Cl in the 2′-position leads to a twisting of the aryl and heterocyclic ring planes (26.32 – 28.49° with mean 27.61°). These molecules form two crystallographically independent *cis*-oid dimers with intra-dimer S⋯S contacts in the range 3.148(2) – 3.335(3) Å (mean 3.240 Å). These S⋯S contacts are, on average, longer than those in **2** [3.156(6) – 3.268(5) Å] which in turn appear a little longer than those in **1** [3.154(2) – 3.235(2) Å]. As with other compounds in this series, **3** adopts a distorted π-stacked structure. In **3** π-stacking along the crystallographic *b*-axis exhibits inter-dimer S⋯S distances falling in the range [4.190(3) – 4.344(2) Å, mean 4.264 Å]. The packing of **3** is similar to, but not isomorphous with, **2**. The *cis*-oid dimers of **3** are linked together in the *ac* plane *via* S⋯Br contacts in the range [3.638(2) – 4.396(2) Å, mean 3.845 Å] forming chains running parallel to the crystallographic *a* axis (Fig. 5), analogous to **2**. These chains are linked *via* a web of C-H⋯Cl, S⋯Cl and C-H⋯N contacts on one side of the molecule, comparable with **2**. The shorter of the S⋯Cl contacts [3.483(2) – 3.732(2) Å, mean

3.595 Å] are comparable with the sum of the van der Waals radii of S and Cl (3.55 Å). Conversely, on the other side of the molecule, the inter-chain S…N contacts in **2** are absent and replaced by S…S contacts. Presumably the loss of these S…N contacts is offset by optimized C-H…Br interactions as well as directional N…Br contacts [3.338(4) – 3.699(4) Å; C-Br⋯N 166.4(2) and 175.6(2)°]. These distances are slightly longer than the directional C-Br⋯N contacts in *p*-BrC$_6$F$_4$CNSSN [GOTQEL, 3.139(9) Å and C-Br⋯N at 162.8(4)°] and BrCNSSN [WASHEE, 3.109(4) Å and C-Br…N at 158.5(1)°].[53,54] Intra and inter-stack contacts are given in Table S4 (ESI).

Figure 5. (top) Solid state structure of **3** in the *ac* plane, highlighting intermolecular S⋯Br and S⋯Cl contacts; (bottom) detail of the chain-forming S…B contacts emphasizing the vertical displacement of molecules with respect to the stacking direction.

Structure of 4. Initial crystallographic studies on **4**, like the other DTDAs presented above, gave a unit cell with a short axis [b = 3.9015(1)Å for **4**]. However, further investigations revealed that a doubling of the b axis generated a supercell equivalent to that of **3**. Subsequent solution and refinement in the super-cell (and including a merohedral twin) revealed that **4** is isomorphous with **3** and crystallizes with four molecules (two crystallographically independent *cis*-oid dimers) in the asymmetric unit. The intra-dimer S⋯S contacts range from 3.12(2) – 3.27(3) Å [mean 3.19 Å] whereas the inter-dimer S⋯S contacts along the π-stacking direction (b axis) span the range 4.58(2) – 4.69(2) Å [mean 4.64 Å]. Conversely both the intra- and inter-dimer I⋯I contacts span 3.78(2) – 4.04(2) (mean 3.91 Å), reflecting a more regular spacing of the substituent groups. The isomorphous nature of compounds **3** and **4** means that the packing of **4** is identical to that of **3**. A set of chain-forming S⋯I contacts propagate parallel to the *a*-axis. range from 3.59(1) – 3.77(1) Å and are comparable with the sum of the van der Waals radii (3.78 Å). The interchain S⋯Cl contact [3.50(2) Å] is comparable with the sum of the van der Waals radii of S and Cl (3.55 Å). The I atom also forms close directional contacts to N [3.35(2) Å] and C-I⋯N angle [161(1)°] analogous to the C-Br⋯N contact in **3**. This distance is comparable to the sum of the van der Waals radii close to the ring plane (3.36 Å).

Magnetic Properties

The variable-temperature magnetic susceptibility (χ) of radicals **1 – 4** was measured using a SQUID magnetometer in an applied field of 0.5 T over the temperature region 5 - 300 K and corrected for both sample diamagnetism (Pascal's constants) and the diamagnetism of the sample holder. Data were collected in both the warming and cooling modes, with no significant differences in sample susceptibility. Plots of χ *vs T* and χT *vs T* for the radical dimer pairs **1 – 4** are shown in Figure 6.

All the radicals are essentially diamagnetic below 150 K, although the χ *vs T* data all reveal a small Curie-tail apparent at low temperatures (Fig. 6a) which is attributed to small numbers of lattice defects which were confirmed by low temperature solid-state EPR studies (*vide infra*). A quantitative fit of the low temperature data reveal defects in the range $\rho = 0.22 – 0.58\%$ for the radical pairs (Table 2). On warming from 150 K to room temperature a steady increase in the susceptibility is observed (Fig. 6a). Examination of the χT data show the onset of paramagnetism occurring earlier for the heavier halo derivatives **3** and **4** (X = Br and I) in relation to the lighter halo radicals **1** and **2** (X = F, Cl). The room temperature χT products for radicals **1 – 4** (0.02, 0.06, 0.05 and 0.07 emu·K·mol^{-1}, respectively) are all substantially less than the value expected for two non-interacting radicals ($C = 0.75$ emu·K·mol^{-1}, assuming $g = 2.0$) but clearly reflect the onset of paramagnetism which is not associated with conventional diamagnetic materials.
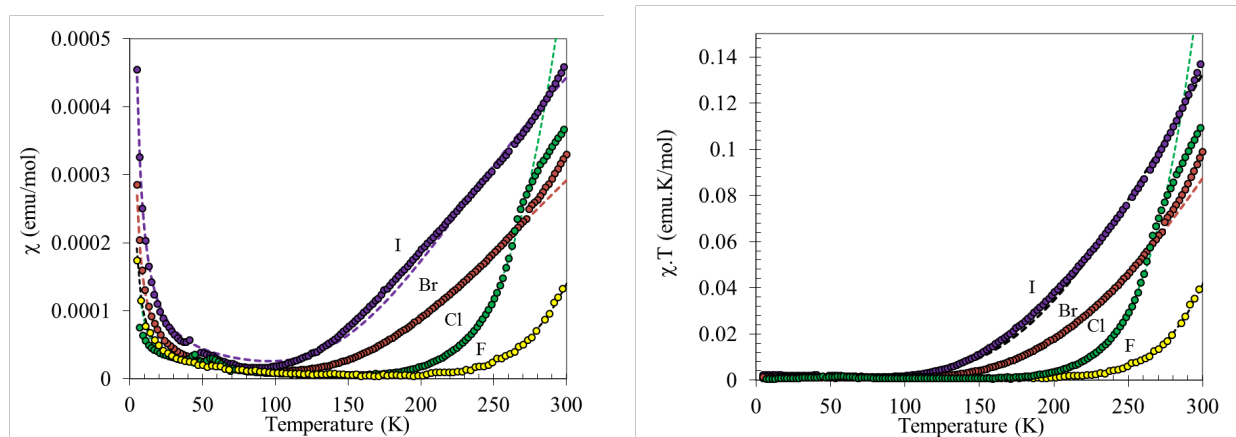
Figure 6. Temperature dependence of (a) χ and (b) χT for radicals **1** (yellow), **2** (green), **3** (brown) and **4** (purple). Dashed lines represent fits to the Bleaney-Bowers model[55] with parameters given in the text and Table 2.

The magnetic data were fitted to the Bleaney-Bowers model[55] to extract the energy gap, $|2J|$, between the ground state singlet and the thermally accessible triplet state. A very good fit was obtained for **3** (to 260 K) and **4** (over the whole temperature region 5 - 300 K) with estimated exchange interactions of $2J \approx -723$ cm^{-1} and $2J \approx -626$ cm^{-1} for radicals **3** and **4** respectively (Table 2). The Bleaney-Bowers model, however, could not fully describe the experimental data for radicals **1** and **2.** Fitting of data for radical **1** up to 240 K gives an exchange interaction of $2J \approx -1223$ cm^{-1} and for radical **2** up to 200 K provides $2J \approx -1112$ cm^{-1} (Fig. S1 and S2 respectively in ESI). These strong antiferromagnetic couplings are consistent with the slightly shorter intra-dimer S⋯S contacts in the crystal structures of these radicals. Structural studies (*vide infra*) show a significant temperature dependence of the intermolecular contacts which may directly affect the overlap integral and hence the exchange coupling J may be temperature or pressure dependent and linked to thermal lattice expansion or contraction.[1,56-58] In addition the presence of increasing numbers of species with $S \neq 0$ within the sample on warming can lead to deviation from the isolated dimer model due to additional exchange coupling between $S = 1$ units along the π-stack (*vide infra*).

Table 2. Intra-dimer S⋯S contacts and fitting parameters to the Bleaney-Bowers model[55] for radical pairs **1 – 4** from SQUID and CW-EPR studies. [Intra-dimer S…S contacts are all reported at 180(2) K except **3** which was measured at 240 K].

Radical	Mean intra-dimer S⋯S contact (Å)	Temp. Range (K)	$2J$ (cm^{-1}) (SQUID)	$2J$ (cm^{-1}) (CW-EPR)	ρ (%)	g
1	3.197(2)	0-230	-1223	---	0.25	2.01
2	3.219(6)	0-200	-1112	-1251	0.22	2.01
3	3.240(3)	0-300	-723	-695	0.35	2.01
4	3.19(2)	0-300	-626	-625	0.58	2.01

Solid-State VT-EPR Studies

DTDAs are generally considered to be diamagnetic. However, we previously showed that for **2** the rise in the susceptibility above 150 K stems from a thermally accessible excited triplet state as a result of a weakened π^*-π^* interaction.[26,27] To unravel the origin of the paramagnetism for radicals **1**, **3** and **4**, variable temperature (VT) continuous wave (CW) X-band EPR studies were carried out on polycrystalline solid samples. We previously showed that the lower temperature (<100 K) EPR spectra for **2** originate from $S = ½$ radical defect centres in the lattice and have the typical hyperfine structure of the isolated radicals (i.e. $g_x = 2.002$, $g_y = 2.008$, $g_z = 2.021$, $^N A_x = 1.4$, $^N A_y < 0.1$, $^N A_z < 0.1$ mT; Fig. S4(A) in ESI).[26] On the other hand, in the high temperature region between 120 and 300 K, the EPR spectra of radicals **1 – 4** are more complex, revealing features that belong to two paramagnetic species; a signal profile for a rhombic $S = 1$ species spread over ca. 50 mT for the $\Delta M_s = \pm 1$ transitions (in addition to the characteristic "forbidden" half-field $\Delta M_s = \pm 2$ transition which can also be detected at low field) and a central narrow signal arising from a rhombic $S = ½$ species due to crystal lattice defects which were also evident at low temperature. For illustrative purposes, a typical wide sweep X-band EPR spectrum of the

radicals (**4**) with these combined $S = \frac{1}{2}$ and $S = 1$ species, is shown in Figure 7 where the characteristic half-field feature is just visible at *ca.* 165 mT.
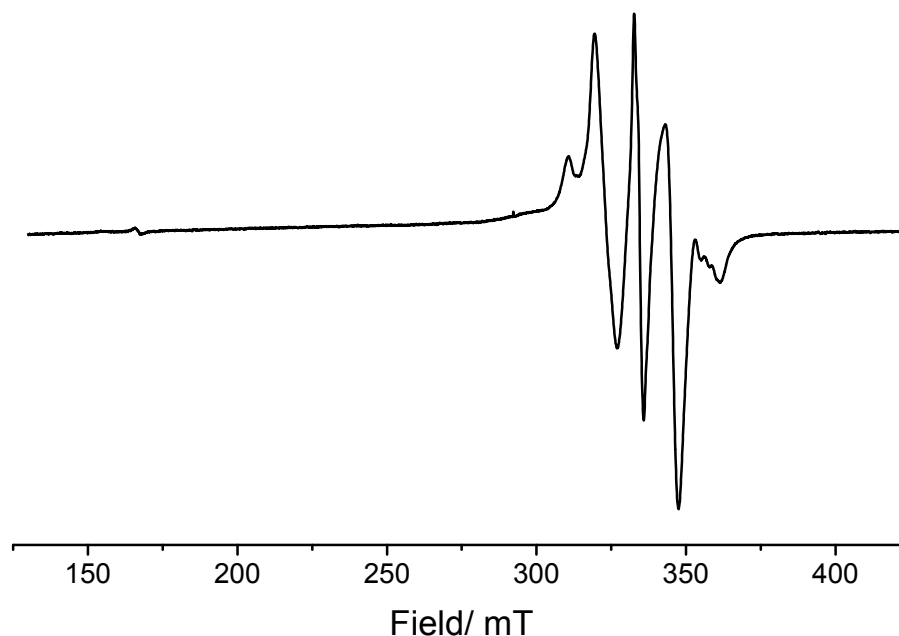
Figure 7. Solid-State CW-EPR spectrum for **4** recorded over a wide-sweep scan range at 190 K.

Representative variable temperature EPR spectra for **3** are shown in Figure 8 where the features around 318 and 345 mT are assigned to the zero field splitting of the triplet state. The intensity of these features initially increases with increasing temperature up to *ca.* 190 K due to increasing thermal population of the excited triplet. With increasing populations of the $S = 1$ state, the average separation of the paramagnetic centres is reduced leading to more prominent dipolar broadening, which depends upon r^{-n}. As a consequence, there is a small thermal window in which the spin-triplets are well resolved. For radical **4**, in the temperature range 120 -160 K, hyperfine structure appears to be additionally superimposed on the fine structure (Fig. S6 in ESI), whilst for radicals **1** and **3** only the inner pair of lines for the triplet signal are clearly observed (Figure 8 and Fig. S3 in ESI); The outer pair of lines corresponding to the D_{zz}

component of the zero-field splitting parameters (ZFS) is poorly resolved and likely due to line broadening arising from unresolved hyperfine coupling to the z-component.
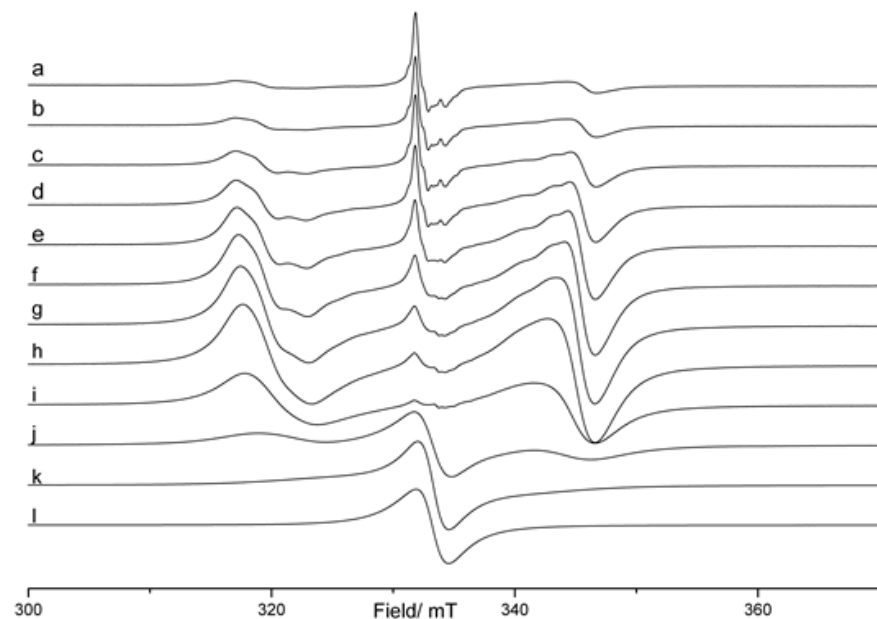
Figure 8. Solid-State VT-EPR spectra for **3** recorded at a) 120, b) 130, c) 140, d) 150, e) 160, f) 170, g) 180, h) 190, i) 200, j) 220, k) 250 and l) 298K.

Simulation of the EPR spectra for **1 – 4** (Fig. 9) required the superposition of spectra arising from two independent paramagnetic species ($S = ½$ and $S = 1$) with a larger linewidth for the outer D_{zz} component compared to the narrower linewidth for the inner D_{xx}, D_{yy} features. The deconvoluted simulations showing the individual contributions from the $S = ½$ and $S = 1$ species in the experimental EPR spectrum are also shown in Figure 9 for **2** (the deconvoluted simulations for **1**, **3** and **4** are given in Figs. S3, S5 and S6 respectively).

The axial ZFS parameter $|D|$ of radicals **1 – 4** (Table 3) appeared to be similar to those observed in other organic π radical dimers.[59-62] For most triplet state organic radicals, the

contribution of spin-orbit coupling to the ZFS is small, and quiet often the **g** anisotropy is small. The ZFS parameters are characterized by the electron-electron dipolar interaction tensor *D*, which gives information on the electron spin distribution and depends inversely on r^3, and the rhombicity parameter *E*, which gives information on the deviation of the electron distribution from axial symmetry. In this case, the rhombicity parameter *E* is very small and this in agreement with the predominantly axial nature of the *D* term expected in these radicals. In other words, the well-defined nature of the SOMO for the radicals, with small *g* anisotropy and large *A* anisotropy, means that the resulting electron-electron dipole interaction in the π*-π* dimer is largely axial.
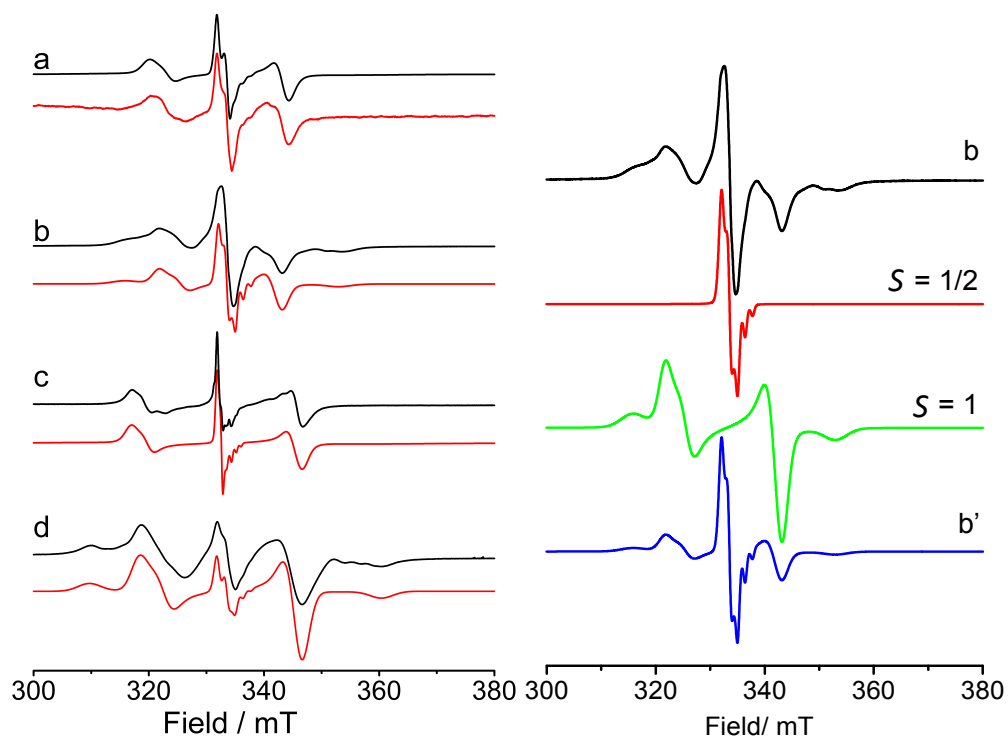
Figure 9. Experimental (red line) and simulated (black line) X-band CW-EPR spectra of polycrystalline samples of: (a) **1** at 220 K; (b) **2** at 220 K; (c) **3** at 140 K and; (d) **4** at 180 K. The

deconvoluted simulation of **2** is also shown, with the $S = \frac{1}{2}$ component (red line), $S = 1$ component (green line) and the combined simulation (blue line, labelled b′).

Table 3. Zero-field splitting parameters extracted from fitting the EPR spectra of radicals **1 – 4** at 220, 220, 140 and 180 K, respectively.

Radical	S	g_{xx}	g_{yy}	g_{zz}	A_x (mT)	A_y (mT)	A_z (mT)	$\lvert D\rvert$ (cm^{-1})	$\lvert E\rvert$ (cm^{-1})
1	½	2.009	2.021	2.002	<0.1	<0.1	1.4		
	1	2.010	2.021	2.002				0.0202	0.0005
2	½	2.008	2.018	2.002	<0.1	<0.1	1.4		
	1	2.010	2.017	2.006				0.0175	0.0009
3	½	2.016	2.021	2.006	<0.1	<0.1	1.4		
	1	2.016	2.020	2.006				0.0255	0.0007
4	½	2.008	2.021	2.002	<0.1	<0.1	1.4		
	1	2.007	2.017	2.002				0.0238	0.0009

The double-integral of the EPR spectrum is proportional to the magnetic susceptibility and EPR can therefore be implemented to determine the singlet-triplet gap of radicals **1 – 4**, providing complimentary data to the SQUID measurements. However, double integration of the $S = 1$ triplet component of the EPR spectra was complicated by the superposition of the $S = \frac{1}{2}$ 'defect' radical signal. Alternatively, analysis of the "forbidden" half-field transition $\Delta M_s = \pm 2$ was difficult since it was not possible to resolve this for all of the radicals examined and so did not provide a consistent methodology across the entire series. We eventually subtracted the integrated intensity of the $S = \frac{1}{2}$ state from the total spectral integration. The temperature dependence of the resulting $S = 1$ state intensity was fitted to the Bleaney-Bowers model to estimate the singlet-triplet gap. However, since the line shape of the two spin systems changes dramatically with temperature, it is difficult to determine the limit of integration for the $S = \frac{1}{2}$ state (especially for the high temperature signals), hence the extracted singlet-triplet gaps should

be treated with a little caution. Good fits were obtained for radicals **2** and **3** and a satisfactory fit for radical **4** with estimated singlet-triplet gaps of -1251, -695 and -625 cm^{-1}, respectively (Fig. 9). These values are in good agreement with the values obtained from the magnetic susceptibility measurements (-1112, -723 and -626 cm^{-1} for radicals **2**, **3** and **4**, respectively). The fitting of the $S = 1$ state EPR intensity for **1** was poor. However, given the good agreement between SQUID data and EPR intensities we feel that the data from the SQUID measurements provides a reliable estimate of J.

(a)   (b)

(c)
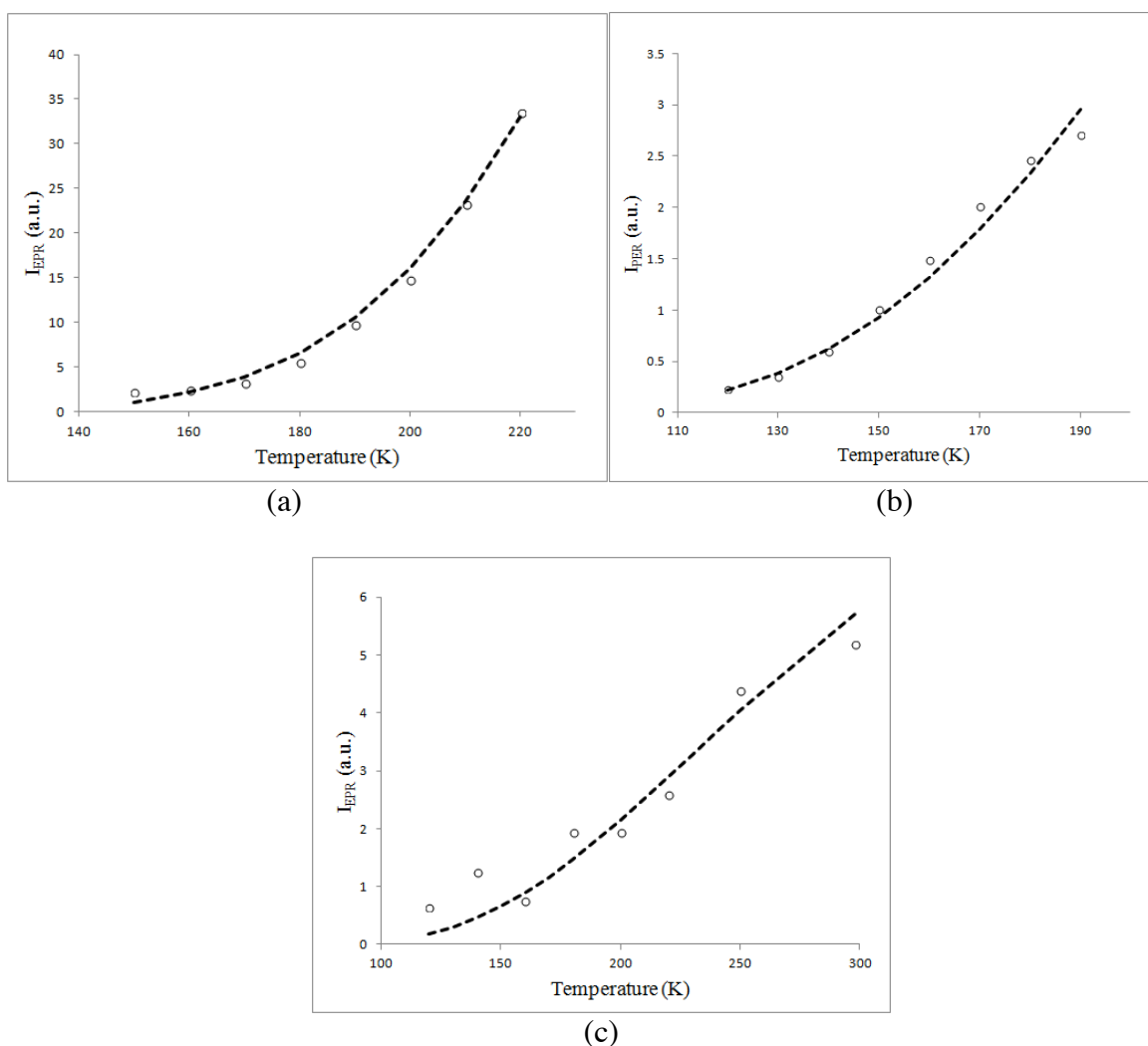
Figure 9. The temperature dependence of the CW-EPR signal intensity of the $S = 1$ state for (a) **2**; (b) **3**; and (c) **4.** Dashed lines represent the best fits to the Bleaney-Bowers model.[55]

From the Boltzmann distribution and the estimated singlet-triplet gaps determined by CW-EPR, we calculated that 0.3, 3.5 and 4.9% of radicals **2**, **3** and **4**, respectively populate the triplet state at room temperature. The high percentage of radicals in the triplet state, especially for radicals **3** and **4,** resulted in the collapse of the fine structure in the EPR resonance lines at 300 K, as dipole-dipole interactions between triplets lead to line broadening. From the estimated singlet-triplet gaps it can also be assumed that the *in situ* dimerization energy of these radicals (half the singlet-triplet gap in the dimer) is *ca*. -15, -8.4 and -7.6 kJ/mol for **2**, **3** and **4**, respectively, significantly lower than the solution dimerization energy determined for $(PhCNSSN)_2$ of *ca*. -35 kJ/mol,[63] but consistent with some other DTDA radicals in the solid state.[23,27]

DISCUSSION

The majority of DTDA radicals form discrete dimer pairs as a consequence of the high favourable dimerization energy.[64] Dimerization typically proceeds *via* multi-centre two electron π^*-π^* interactions between the out-of-phase components of the two singly-occupied molecular orbitals (SOMOs) (Fig. 1).[64,65] This interaction stabilizes the singlet ground state which is experimentally supported by χT values ~ 0 emu.K.mol^{-1} at low temperature.[26-29] Passmore was the first to indicate that the "closed-shell" dimerization of DTDA radicals inadequately described the electronic ground state of these materials and that they had some diradical character,[23] more recently studied computationally by Kertesz.[24] This behaviour has also been observed in other thiazyl radicals.[66] Passmore and co-workers indicated that radical pairs with singlet-triplet energy gaps between -500 to 2000 cm^{-1} would have triplet excitons that could be detected by EPR.[29] The DTDA radical pair $[NC(CF_2)_4CNSSN]_2$ (COHJOZ) was shown to have an experimentally

detected triplet excited state with a singlet-triplet gap of -1730 cm^{-1} as determined by EPR (or 2J = -1500 cm^{-1} by magnetic susceptibility measurements) and 35% diradicaloid character calculated at the CASSCF(6,6)/6-31G* level of theory.[29] It should be noted that the intra-dimer distances in the *trans*-cofacial dimers of this radical are *ca.* 3.20 – 3.26 Å. This is slightly longer than what is normally observed for other DTDA derivatives,[64,65] but similar to the intra-dimer distances of radicals **1** – **4** (Table 2). The longer intra-dimer distances in these radicals result in smaller overlap integrals, weaker exchange couplings and the energy of the excited triplet state falls and becomes thermally accessible. Such elongated bonds have been observed in other dimers such as those based on phenalenyl,[60,67] tetrathiafulvalenium (TTF$^{+\bullet}$)[61,68] and tetracyanoethylenide (TCNE$^{\bullet-}$)[59,69-71] radicals with magnetic exchange coupling less than 2000 cm^{-1} and thermally accessible triplet excitons.

Both steric and electronic effects can potentially contribute to weakening of the π*-π* dimer interaction. Previous electrochemical studies by Banister and Boeré have shown that the electronic properties of aryl DTDA radicals show only a slight substituent dependency.[37,72,73] The diagnostic g-value and hyperfine coupling to N similarly reflect limited electronic tuning of the SOMO.[65] Conversely the substituents clearly have an effect on dimer packing motifs which have been explored through molecular electrostatic potential maps.[49,51,52] MEPs for **1** – **4** are presented in Figure 10 with red reflecting areas repulsive to a point positive charge and blue reflecting areas attractive to a point positive charge.

Figure 10. Molecular electrostatic isopotentials for **1 – 4** (surfaces plotted at 20 kcal.mol^{-1})

For **1** and **2** the largest positive charge is associated with the disulfide bond whereas in **3** and **4** the softer halogens offer alternative effective regions of positive charge. All four radicals exhibit negative charges in the vicinity of the N lone pairs. Thus **1** and **2** exhibit S…N contacts to this electronegative 'pocket'. Conversely the heavier halogens build up regions of electropositive character favoring structure-directing N$^{\delta-}$…Br$^{\delta+}$ and N$^{\delta-}$…I$^{\delta+}$ contacts between the soft, polarizable halogen and the harder polarizing N.

To date, weakening of the dimerization in DTDA radicals has been achieved through the use of groups (F, CF$_3$, Me) in the 2′/6′-positions to weaken π*-π* dimerization (GOTQEL, HAKYOI, HAWRAZ, ILUKIJ, YOMXUT).[1,2,11-13,76] In many of these cases dimerization was entirely overcome. Our recent studies implemented the propensity of chlorinated aromatics to adopt a π-stacked "β-sheet" structure in which the short-axis (corresponding to the π-stacking direction) falls in the range 3.8 – 4.0 Å (mean 3.9 Å).[50] These inter-molecular contacts are substantially longer than the typical intra-dimer contacts in derivatives of DTDA radicals (mean 3.1 Å) leading to a build-up of strain due to the competing nature of these intermolecular forces. The structural data for the previously reported Cl$_2$C$_6$H$_3$CNSSN$^\bullet$ derivatives[26-28] (DIXMII, DIXMOO, DIXNAB. DIXNEF, MEJZIL) reveals a weakening of the dimerization enthalpy as the intra-dimer S⋯S contacts increases. In the current study, systematic replacement of the halogen at the 5′ position leads to a general increase in the intra-dimer S⋯S distances with increasing size of the halogen (though we note that the large esds associated with the structure of **4** provide significant uncertainty in this trend) and this is directly reflected in weaker magnetic exchange. Within a

localized bonding approach it can be shown that the strength of the exchange coupling in the weak overlap limit is directly proportional to the overlap integral, S, according to Eq. 1:[77]

$$2J = 2K - 4S\beta \hspace{4cm} \text{Eq. 1}$$

where K is the potential exchange integral which is a manifestation of Hund's Rules and favors coparallel spin alignment whereas the term $-4S\beta$ relates to the overlap integral S and β is the resonance integral and stabilizes an antiferromagnetic ground state.[77] This second term is particularly appropriate within the context of these DTDA radicals and other 'pancake' bonded dimers[35] where the overlap integral (S) is low and the ground state configuration cannot be described in terms of a classical (multi-center) covalent bond but has some diradical character.

It is noteworthy that the magnetic properties of **2** deviates significantly from the simple S = ½ dimer model of Bleaney and Bowers above *ca*. 270 K whereas **4**, despite exhibiting a stronger paramagnetic response across the temperature range, follows the Bleaney-Bowers model throughout the temperature range studied. In order to more fully understand the behavior of these dimers we have undertaken detailed variable temperature crystallographic studies on both **2** and **4**. We commence with a discussion of **4** before discussing the more complex case of radical **2**.

Structural studies on **4** were undertaken on the same single crystal across the temperature range 140 – 300 K with full data sets collected at 140 K, 220 K, 240 K, 260 K, 280 K and 300 K. in all cases structure solution and refinement proceeded smoothly in the orthorhombic space group Pna2$_1$ with some small modifications in unit cell parameters expected upon warming. Figure 11 shows the marked increase in intra-dimer S…S contacts on warming and the corresponding decrease in inter-dimer S…S contacts such that there is a general convergence

towards a regular π-stacked structure on warming. In this context the expected inter-radical spacing for a regular π-stack corresponds to $b/2$ and is included in Figure 11 for comparison. Although both of the two crystallographically independent dimers move towards a regular π-stacked motif, the rate at which they do so significantly differs. The dimer containing $S(11)/S(12)/S(21)/S(22)$ responds more abruptly to temperature changes. In contrast both the Cl…Cl and I…I contacts along the stacking direction are more regular (Cl..Cl ranging from 3.747(3) to 4.032(3) Å at 140 K to 3.876(7) – 4.027(7) Å at 300 K; I…I ranging from 3.855(1) – 3.906(1) at 140 K to 3.934(2) – 3.961(2) Å at 300 K). An examination of the thermal parameters for the 140 and 300 K structures reveal that the DTDA ring undergoes significant dynamic motion at 300 K corresponding to displacements of the ring along the stacking direction. This process appears to commence at 220 K with $S(21)$ and, by 300 K, all sulfur atoms show significantly elongated thermal displacement parameters (Figure 11).
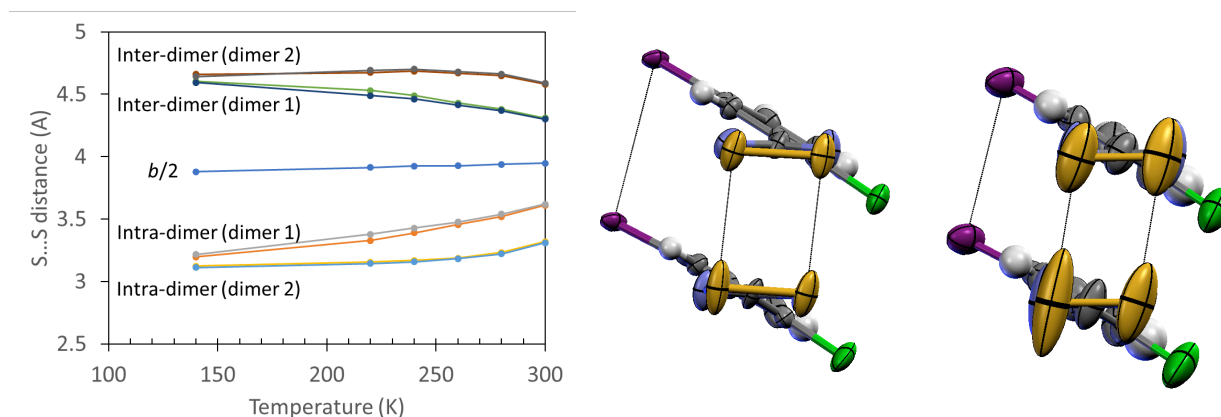
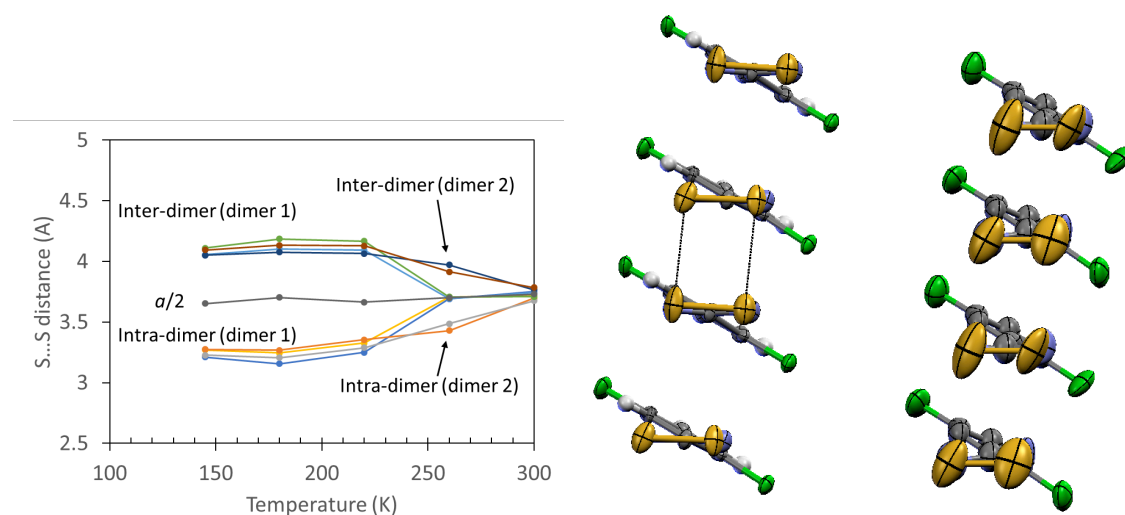
Figure 11. (left) Temperature dependence of the intra-dimer and inter-dimer S…S contacts in **4** in relation to half the crystallographic b-axis (π-stacking direction); thermal ellipsoids are shown (80% probability) for the same crystallographically unique dimer at 140 K (center) and 300 K (right).

A second set of variable temperature studies were undertaken on radical **2**. In this case the temperature dependence of the crystallography proved significantly more problematic. At low temperature the unit cell compared well with the literature data but at ambient temperature the essential disappearance of the $h = 2n + 1$ lines favored an apparent halving of the a-axis. Between 220 K and 260 K these $h = 2n + 1$ reflections change from being well defined peaks to a region of diffuse scattering which continued to fade as the temperature is further raised (Figure 12). Nevertheless with some diffuse scattering in this region still observed, all data sets were integrated in the original cell. A summary of the crystallographic parameters are presented in Table S.1 of the ESI.
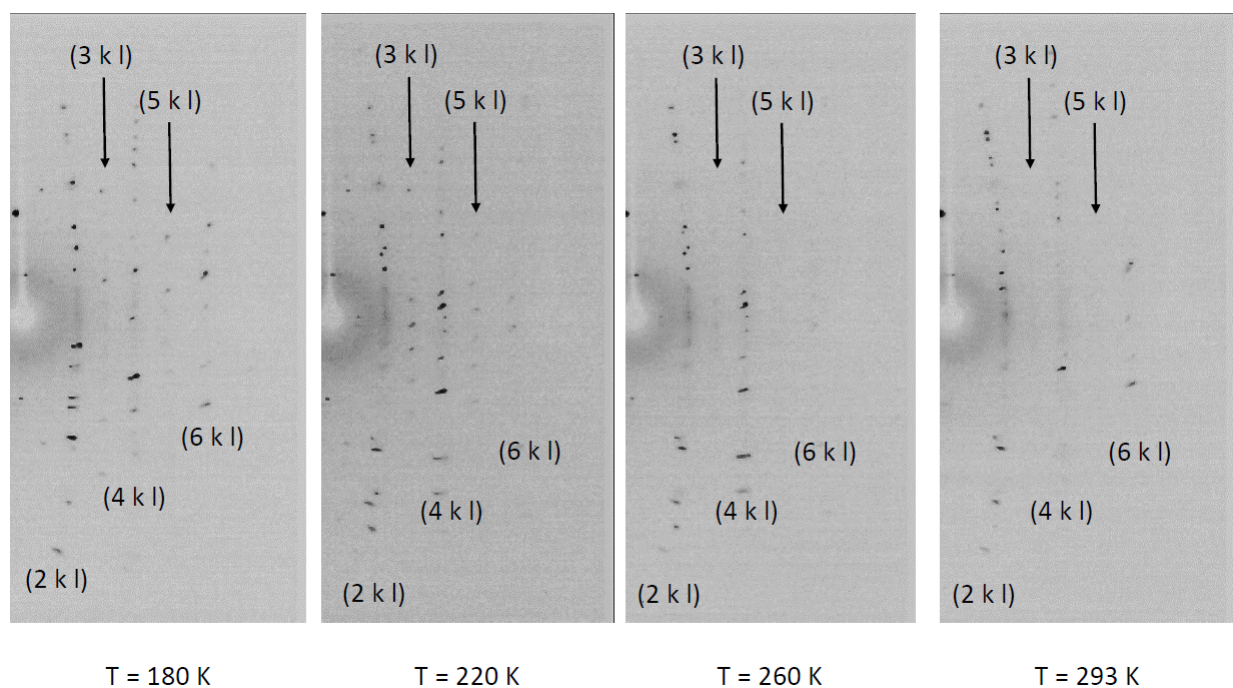
Figure 12. Diffraction pattern (Mo-Kα) from a crystal of **2** in the same orientation measured from 180 to 293 K, illustrating the disappearance of the highlighted $h = 2n + 1$ supercell reflections on warming.

Unlike **4** which exhibits a monotonic change in the intra- and inter-dimer S….S distances along the stacking direction, compound **2** exhibits a structural discontinuity between 220 K and 260 K consistent with a move from an irregular stacking pattern to a more regular π-stacked motif (Figure 13). A close examination of the intra- and inter-dimer S…S contacts along the stacking direction reflect subtle difference between the processes involved for the two crystallographically independent dimers in the unit cell.

Figure 13. (left) Temperature dependence of the intra-dimer and inter-dimer S…S contacts in **2** in relation to half the crystallographic *a*-axis (π-stacking direction); thermal ellipsoids (80% probability) for the same crystallographically unique dimer at 145 K (center) and 300 K (right).

For dimer 1 (containing S11, S12, S21, S22) the transition appears abrupt with the S…S contacts moving from an alternating 3Å/4Å repeat along the *a*-axis at 220 K to a near regular 3.6 Å repeat distance at 260 K. Conversely the second crystallographically independent dimer continues to follow the smooth second-order trend evident in the iodo system, **4** (compare Fig. 11). Unlike **4**, convergence in the S…S separation for both dimer pairs with half the crystallographic *a*-axis is

essentially complete at 300 K, such that the structure might better be described in terms of a regular π-stack motif at ambient temperature. This evolution in structure over the 220 – 300 K range is likely the source of the significant discrepancy in the magnetism of these 'dimers' on approaching ambient temperature which is particularly pronounced for **2** (Fig. 6a). Such regularly spaced radical stacks would better be described as a 1-D Heisenberg chain of S = ½ spins in the high temperature limit.

CONCLUSIONS

The current study illustrates how systematic substitution can be used to study orbital overlap effects on the strength of intra-dimer exchange coupling. These results confirm that these multi-centre π^*-π^* interactions cannot be regarded as purely closed shell configurations, but retain some diradical character. Although all structures comprise a distorted π-stack at low temperature, replacement of halogens in the 5′ position play a role in perturbing the π-stacked structure common to this series. The detailed variable temperature structural studies reveal evidence for significant thermal motion along the stacking direction. Such dynamic behavior has been proposed to be responsible for the magnetic -structural behavior of other thiazyl radicals.[78,79] A careful examination of the intra-dimer and inter-dimer S…S contacts in **4** clearly reflect a gradual transition from a distorted low temperature π-stacked structure towards a more regular π-stacked motif on warming to room temperature, though even at room temperature the structure lies some way from a regular stacked motif. Conversely the supercell ($2n+1\ k\ l$) reflections for **2**, which are clearly evident at 140 K, lose intensity on warming towards ambient temperature. In the case of **2**, a regular π-stacked motif is essentially generated at 300 K with one of the two crystallographically independent dimers following a gradual structural change to a regular stack

whereas the second dimer undergoes a more abrupt transition between 220 and 260 K, with an essentially complete disappearance of supercell reflections between 260 and 293 K, consistent with formation of a regular π-stacked structure. This dynamic process is reflected in the magnetic data which reflect a move away from classical isolated dimer pairs. The thermal evolution from distorted towards regular π-stacking in these DTDA radicals is in contrast to the discontinuous processes evident for a series of 1,3,2-dithiazolyl radicals.[80-85]

ASSOCIATED CONTENT

X-Ray crystallographic information file (CIF) is available for radicals **1**, **3** and **4** and variable temperature studies on both **2** and **4**. Magnetic susceptibility data and solid-state variable temperature CW-EPR measurements for **1 − 4**. This material is available free of charge via the Internet at http://pubs.acs.org.

AUTHOR INFORMATION

Corresponding Author

*E-mail: Christos.Constantinides@uwindsor.ca

Notes

The authors declare no competing financial interest.

ACKNOWLEDGMENTS

REFERENCES

1. Thomson, R.I.; Pask, C.M.; Lloyd, G.O.; Mito, M.; Rawson, J.M. *Chem. Eur. J.*, **2012**, *18*, 8629 – 8633.

2. Alberola, A.; Less, R.J.; Pask, C.M.; Rawson, J.M.; Palacio, F.; Oliete, P.; Paulsen, C.; Yamaguchi, A.; Farley, R.D.; Murphy, D.M. *Angew. Chem. Int.Ed.*, **2003**, *42*, 4782 – 4785.

3. Wu, J.; MacDonald, D. J.; Clérac, R.; le-Rang, J.; Jennings, M.; Lough, A. J.; Britten, J.; Robertson, C.; Dube, P. A.; Preuss, K. E. *Inorg. Chem.* **2012**, *51*, 3827 – 3839.

4. Hearns, N. G. R.; Hesp, K. D.; Jennings, M.; Korčok, J. L.; Preuss, K. E.; Smithson, C. S. *Polyhedron*, **2007,** *26*, 2047 – 2053.

5. Britten, J.; Hearns, N. G. R.; Preuss, K. E.; Richardson, J. F.; Bin-Salamon, S. *Inorg. Chem.* **2007**, *46*, 3934 – 3945.

6. Preuss, K. E. *Dalton Trans.* **2007**, 2357 – 2369.

7. Jennings, M.; Preuss, K. E.; Wu, J. *J. Chem. Soc., Chem. Comm.* **2006**, 341 – 343.

8. Fatila, E. M.; Maahs, A. C.; Mills, M. B.; Rouzières, M.; Soldatov, D. V.; Clérac, R.; Preuss, K. E. *Chem. Commun.* **2016**, *52*, 5414 – 5417.

9. Fatila, E. M.; Mayo, R. A.; Rouzières, M.; Jennings, M. C.; Dechambenoit, P.; Soldatov, D. V.; Mathonière, C.; Clérac, R.; Coulon, C.; Preuss, K. E. *Chem. Mater.* **2015**, *27*, 4023 – 4032.

10. Mills, M. B.; Hollingshead, A. G.; Maahs, A. C.; Soldatov, D. V.; Preuss, K. E. *CrystEngComm.* **2015**, *17*, 7816 – 7819.

11. Beekman, R.A.; Boeré, R.T.; Moock, K.H.; Parvez, M. *Can. J. Chem.*, **1998**, *76*, 85 – 93.

12. Alberola, A.; Less, R.J.; Palacio, F.; Pask, C.M.; Rawson, J.M. *Molecules*, **2004**, *9*, 771 – 781.

13. Alberola, A.; Clarke, C.S.; Haynes, D.A.; Pascu, S.I.; Rawson, J.M. *Chem.Commun.*, **2005**, 4726 – 4727.

14. Barclay, T.M.; Cordes, A.W.; George, N.A.; Haddon, R.C.; Itkis, M.E.; Oakley, R.T. *Chem.Commun.* **1999**, 2269 – 2270.

15. Beldjoudi, Y.; Arauzo, A.; Palacio, F.; Pilkington, M.; Rawson, J.M. *J. Am. Chem.Soc.*, **2016**, *138*, 16779 – 16786.

16. Fatila, E.M.; Jennings, M.C.; Goodreid, J.; Preuss, K.E. *Acta Cryst.*, **2010**, *C66*, o260.

17. Domagała, S.; Haynes, D.A. *CrystEngComm.*, **2016**, *18*, 7116 – 7125.

18. Domagała, S.; Kosc, K.; Robinson, S.W.; Haynes, D.A.; Woźniak, K. *Cryst. Growth Des.*, **2014**, *14*, 4834 – 4848.

19. Vegas, A.; Pérez-Salazar, A.; Banister, A. J.; Hey, R. G. *J. Chem. Soc., Dalton Trans.* **1980**, 1812 – 1815.

20. Gillespie, R. J.; Kent, J. P.; Sawyer, J. F. *Inorg. Chem.* **1981**, *20*, 3784 – 3799.

21. Gleiter, R.; Bartetzko, R.; Hofmann, P. *Z. Naturforsch.* **1980**, *B35*, 1166 – 1170.

22. Gleiter, R.; Haberhauer, G. *J. Org. Chem.* **2014**, *79*, 7543 – 7552.

23. Decken, A.; Cameron, T. S.; Passmore, J.; Rautiainen, J. M.; Reed, R. W.; Shuvaev, K. V.; Thompson, L. K. *Inorg. Chem.* **2007**, *46*, 7436 – 7457.

24. Beneberu, H. Z.; Tian, Y.-H.; Kertesz, M. *Phys. Chem. Chem. Phys.* **2012**, *14*, 10713 – 10725.

25. Melen, R.L.; Less, R.J.; Pask, C.M.; Rawson, J.M. *Inorg. Chem.*, **2016**, *55*, 11747 – 11759.

26. Constantinides, C. P.; Eisler, D. J.; Alberola, A.; Carter, E.; Murphy, D. M.; Rawson, J. M. *CrystEngComm.* **2014**, *16*, 7298 – 7312.

27. Beldjoudi, Y.; Haynes, D. A.; Hayward, J. J.; Manning, W. J.; Pratt, D. R.; Rawson, J. M. *CrystEngComm.* **2013**, *15*, 1107 – 1113.

28. Alberola, A.; Carter, E.; Constantinides, C. P.; Eisler, D. J.; Murphy, D. M.; Rawson, J. M. *Chem.Commun.* **2011**, 2532 – 2534.

29. Shuvaev, K.V.; Decken, A.; Grein, F.; Abedin, T. S. M.; Thompson, L. K.; Passmore, J. *Dalton Trans.* **2008**, 4029 – 4037.

30. Fehér, F., "Dichloromonosulfane", In *Handbook of Preparative Inorganic Chemistry*, 2nd Ed.; Brauer, G. Ed.; Academic Press, **1963**, NY. Vol. 1, 370 – 371.

31. Stoll, S.; Schweiger, A. *J. Magn. Reson.* **2006**, *178*, 42 – 55.

32. SHELXTL version 6.12, Bruker AXS, Madison, Wisconsin, USA, **2001**.

33. Macrae, C. F.; Edgington, P. R.; McCabe, P.; Pidcock, E.; Shields, G. P.; Taylor, R.; Towler, M.; van de Streek, J. *J. Appl. Crystallogr*. **2006**, *39*, 453 – 457.

34. Beer, L.; Cordes, A. W.; Myles, D. J. T.; Oakley, R. T.; Taylor, N. J. *CrystEngComm*., **2000**, *2*, 109 – 114.

35. Preuss, K. E. *Polyhedron* **2014**, *79*, 1 – 15.

36. Nyburg, S. C.; Faerman, C. H. *Acta Cryst*., **1985**, *B41*, 274 – 279.

37. Boeré, R. T.; Moock, K. H.; Parvez, M. *Z. Anorg. Allg. Chem*. **1994**, *620*, 1589 – 1598.

38. Hazell, A. C.; Hazell, R. T. *Acta Cryst*.**1988**, *C44*, 1807 – 1810.

39. Andreasen, O.; Hazell, A.C.; Hazell, R.G. *Acta Cryst*. **1977**, *B33*, 1109 – 1112.

40. Hofs, H.-U.; Bats, J.W.; Gleiter, R.; Hartmann, G.; Mews, R.; Eckert-Maksic, M.; Oberhammer, H.; Sheldrick, G.M.; *Chem.Ber*. **1985**, *118*, 3781 – 3804.

41. Smith, J.N.B.; Rawson, J.M.; Davies, J.E. *Acta Cryst*. **1999**, *C55*, 1330 – 1332.

42. Gelbrich, T.; Humphries, M.; Hursthouse, M.B.; Ramsden, C.A. *ARKIVOC* **2002**, *3*, 224 – 226.

43. Britten, J.F.; Cordes, A.W.; Haddon, R.C.; Itkis, M.E.; Oakley, R.T.; Reed, R.W.; Robertson, C.M. *CrystEngComm*. **2002**, *4*, 205 – 207.

44. Banister, A.J.; Clegg, W.; Hauptman, Z.V.; Luke, A.W.; Wait, S.T. *Chem.Commun*. **1989**, 351 – 352.

45.   Clegg, W.; Birkby, S.L.; Banister, A.J.; Rawson, J.M.; Wait, S.T.; Rizkallah, P.; Harding, M.M.; Blake, A.J. *Acta Cryst*. **1994**, *C*50, 28 – 33.

46.   Tschope, P.; Rademacher, O.; Bottcher, P. *Z.Kristallogr*. **1998**, *213*, 123 – 129.

47.   Scholz, U.; Roesky, H.W.; Schimkowiak, J.; Noltemeyer, M. *Chem.Ber*. **1989**, *122*, 1067 – 1070.

48.   Ruangsuttinarupap, S.; Gross, H.-D.; Willing, W.; Muller, U.; Dehnicke, K. *Z.Anorg.Allg.Chem*. **1986**, *536*, 153 – 163.

49.   Clarke, C. S.; Haynes, D. A.; Smith, J. N. B.; Batsanov, A. S.; Howard, J. A. K.; Pascu, S. I.; Rawson, J. M. *CrystEngComm*. **2010**, *12*, 172 – 185.

50.   Desiraju, G. R. *Crystal Engineering: The Design of Organic Solids*; Materials Science Monographs, 54, Elsevier Press, 1989.

51.   Haynes, D.A. *CrystEngComm*, **2011**, *13*, 4793 – 4805.

52.   Bond, A.D.; Haynes, D.A.; Pask, C.M.; Rawson, J.M. *J.Chem.Soc.,Dalton Trans*. **2002**, 2522 – 2531.

53.   Antorrena, G.; Davies, J.E.; Hartley, M.; Palacio, F.; Rawson, J.M.; Smith, J.N.B.; Steiner, A. *Chem.Commun*., **1999**, 1393 – 1394.

54.   Knapp, C.; Lork, E.; Gupta, K.; Mews, R. *Z.Anorg.Allg.Chem*. **2005**, *631*, 1640 – 1644.

55.   Bleaney, B.; Bowers, K. D. *Proc. R. Soc. London, Ser. A* **1952**, *214*, 451 – 465.

56. Kahn, O.; Morgenstern-Badarau, I.; Audiere, J. P.; Lehn, J. M.; Sullivan, S. A. *J. Am. Chem. Soc.* **1980**, *102*, 5935 – 5936.

57. Sheppard, C. L.; Tandon, S. S.; Thompson, L. K.; Bridson, J. N.; Miller, D. O.; Handa, M.; Lloret, F. *Inorg. Chim. Acta* **1996**, *250*, 227 – 239.

58. Muthukumaran, R.; Chandramouli, G. V. R.; Manoharan, P. T. *Chem. Phys. Lett.* **2005**, *404*, 227 – 231.

59. Miller, J. S.; Novoa, J. J. *Acc. Chem. Res.* **2007**, *40*, 189 – 196.

60. Mou, Z.; Uchida, K.; Kubo, T.; Kertesz, M. *J. Am. Chem. Soc.*, **2014**, *136*, 18009 – 18022.

61. Fumanal, M.; Capdevila-Cortada, M.; Miller, J.S.; Novoa, J.J. *J. Am. Chem. Soc.*, **2013**, 135, 13814 – 13826.

62. Tian, Y.-H.; Kertesz, M. *J. Phys. Chem. A*, **2011**, *115*, 13942 – 13949.

63. Fairhurst, S.A.; Johnson, K.M.; Sutcliffe, L.H.; Preston, K.F.; Banister, A.J.; Hauptman, Z.V.; Passmore, J. *J. Chem. Soc., Dalton Trans.*, **1986**, 1465 – 1472.

64. Rawson, J. M.; Alberola, A.; Whalley, A. *J. Mater. Chem.* **2006**, *16*, 2560 – 2575.

65. Rawson, J.M.; Banister, A.J. and Lavender, I, *Adv. Heterocycl. Chem.*, **1995**, *62*, 137 – 247.

66. Cameron, T.S.; Decken, A.; Kowalczyk, R.M.; McInnes, E.J.L.; Passmore, J.; Rawson, J.M.; Shuvaev, K.V.; Thompson, L.K. *Chem. Commun.*, **2006**, 2277 – 2279.

67. Goto, K.; Kubo, T.; Yamamoto, K.; Nakasuji, K.; Sato, K.; Shiomi, D.; Takui, T.; Kubota, M.; Kobayashi, T.; Yakushi, K.; Ouyang, J. *J. Am. Chem. Soc.* **1999**, *121*, 1619-1620.

68. Guirauden, A.; Johannsen, I.; Batail, P. Coulon, C. *Inorg. Chem.* **1993**, *32*, 2446 – 2452.

69. Olmsted, M. M.; Speier, G.; Szabo, L. *J. Chem.Soc., Chem.Commun.* **1994**, 541 – 543.

70. Johnson, M.J.; Campana, C.; Foxman, B.M.; Desmarais, W.; Vela, M. J.; Miller, J. S. *Chem.Eur.J.* **2000** , *6*, 1805 – 1810.

71. DelSesto, R.E.; Botoshansky, M.; Kaftory,M.; Miller,J.S. *CrystEngComm.* **2002**, *4*, 106 – 108.

72. Aherne, C.M.; Banister, A.J.; Gorrell, I.B.; Hansford, M.I.; Hauptman, Z.V.; Luke, A.W.; Rawson, J.M., *J. Chem. Soc., Dalton Trans.*, **1993**, 967 – 972;

73. Aherne, C.M.; Banister, A.J.; Hibbert, T.G.; Luke, A.W.; Rawson, J.M. *Polyhedron*, **1997**, 16, 4239 – 4245.

74. Banister, A.J.; Bricklebank, N.; Clegg, W.; Elsegood, M.R.J.; Gregory, C.I.; Lavender, I.; Rawson, J.M.; Tanner, B.K. *J. Chem. Soc., Chem. Commun.*, **1995**, 679 – 680.

75. Banister, A.J.; Bricklebank, N.; Lavender, I.; Rawson, J.M.; Gregory, C.I.; Tanner, B.K.; Clegg, W.; Elsegood, M.R.J.; Palacio, F. *Angew. Chem., Int Ed.*, **1996**, *35*, 2533 – 2535.

76. Beekman, R.A.; Boeré, R.T.; Moock, K.H.; Parvez, M. *Can.J.Chem.*, **1998**, *76*, 85 – 93.

77. Equation 1 holds in the case of poor spatial overlap where the higher order term in the overlap integral $2S^2(2\alpha + j)$ can be neglected. See: Kahn, O., *Molecular Magnetism*, VCH

1993, p.152. Note equation 1 defines the singlet-triplet gap as $2J$ consistent with the Hamiltonian $H = -2JS_1S_2$ whereas Kahn defines this gap as J.

78. Vela, S.; Deumal, M.; Shiga, M.; Novoa, J.J.; Ribas-Arino, J. *Chem. Sci.*, **2015**, *6*, 2371 – 2381.

79. Vela, S.; Mota, F.; Deumal, M.; Suizu, R.; Shuku, Y.; Mizuno, A; Awaga, K; Shiga, M.; Novoa, J.J.; Ribas-Arino, J. *Nature Comm*. **2014**, *5*, 4411.

80. Brusso, J.L.; Clements , O.P.; Haddon, R.C.; Itkis, M.E.; Leitch, A.A.; Oakley, R.T.; Reed, R.W.; Richardson, J.F. *J. Am. Chem. Soc.*, **2004**, *126*, 14692–14693.

81. Brusso, J.L.; Clements, O.P.; Haddon, R.C.; Itkis, M.E.; Leitch, A.A.; Oakley, R.T.; Reed, R.W.; Richardson, J.F. *J. Am. Chem. Soc.*, **2004**, *126*, 8256 – 8265.

82. Fujita, W.; Awaga, K. *Science*, **1999**, *286*, 261 – 262;

83. McManus, G.D.; Rawson, J.M.; Feeder, N.; van Duijn, J.; McInnes, E.J.L.; Novoa, J.J.; Burriel, R.; Palacio, F.; Oliete, P. *J. Mater. Chem.*, **2001**,*11*, 1992 – 2003.

84. Alberola, A.; Collis, R.J.; Humphrey, S.M.; Less, R.J.; Rawson, J.M. *Inorg. Chem.*, **2006**, *45*, 1903 – 1905.

85. Alberola, A.; Burley, J.; Collis, R.J.; Less, R.J.; Rawson, J.M., *J. Organmet. Chem.* **2007**, *692*, 2750-2760.

Effects of Halo-substitution on 2′-Chloro-5′-halo-phenyl-1,2,3,5-dithiadiazolyl Radicals: A Crystallographic, Magnetic and EPR Case Study

C.P. Constantinides, E. Carter, D. Eisler, Y. Beldjoudi, D.M. Murphy and J.M. Rawson.
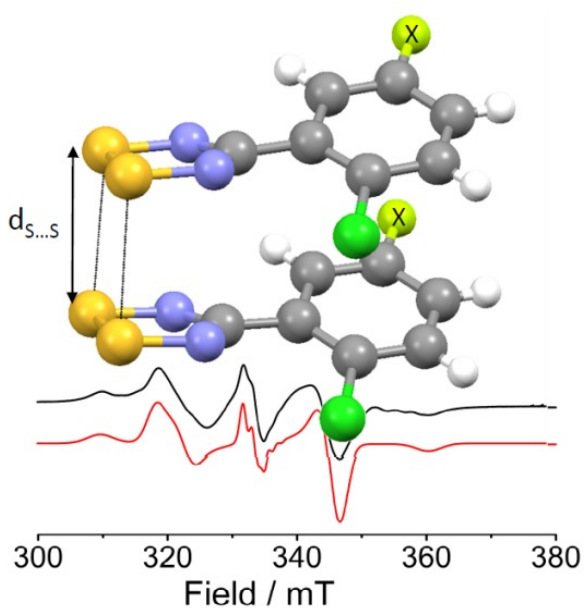
Synopsis: We report a detailed variable-temperature (VT) crystallographic, magnetic and EPR study of a series of halogenated 1,2,3,5-dithiadiazolyl radicals which exhibit singlet ground states and thermally accessible low-lying triplet states. Structural studies reveal a progression from a distorted π-stack at low temperature towards a regular π-stack at high temperature.